Lattice QCD Study of Pion Electroproduction and Weak Production from a Nucleon

Yu-Sheng Gao,[1] Zhao-Long Zhang,[1] Xu Feng,[1,2,3,*] Lu-Chang Jin,[4,†] Chuan Liu,[1,2,3] and Ulf-G. Meißner[5,6,7]

[1]*School of Physics, Peking University, Beijing 100871, China*
[2]*Collaborative Innovation Center of Quantum Matter, Beijing 100871, China*
[3]*Center for High Energy Physics, Peking University, Beijing 100871, China*
[4]*Department of Physics, University of Connecticut, Storrs, Connecticut 06269, USA*
[5]*Universität Bonn, Helmholtz-Institut für Strahlen- und Kernphysik and Bethe Center for Theoretical Physics, D-53115 Bonn, Germany*
[6]*Forschungszentrum Jülich, Institute for Advanced Simulation (IAS-4), D-52425 Jülich, Germany*
[7]*Peng Huanwu Collaborative Center for Research and Education, International Institute for Interdisciplinary and Frontiers, Beihang University, Beijing 100191, China*

(Received 18 February 2025; revised 30 March 2025; accepted 15 April 2025; published 30 April 2025)

Quantum fluctuations in QCD influence nucleon structure and interactions, with pion production serving as a key probe of chiral dynamics. In this Letter, we present a lattice QCD calculation of multipole amplitudes at threshold, related to both pion electroproduction and weak production from a nucleon, using two gauge ensembles near the physical pion mass. We develop a technique for spin projection and construct multiple operators for analyzing the generalized eigenvalue problem in both the nucleon-pion system in the center-of-mass frame and the nucleon system with nonzero momentum. The numerical lattice results are then compared with those extracted from experimental data and predicted by low-energy theorems incorporating one-loop corrections.

DOI: 10.1103/PhysRevLett.134.171904

Introduction—Quantum fluctuations are fundamental to modern physics, shaping many key phenomena. In QCD, gluon field fluctuations are key to quark confinement and asymptotic freedom. In the nonperturbative regime, they influence quark and gluon dynamics within nucleons, affecting their distributions and interactions. These effects, in turn, shape how nucleons respond to external probes like photons and weak bosons. When energy allows, quantum fluctuations can manifest as real particles, such as pions, in electroproduction and weak production. Pion production is of particular interest, as pions, being Nambu-Goldstone boson of QCD, reflect spontaneous chiral symmetry breaking and play a crucial role in chiral dynamics (see, e.g., [1]).

The study of pion production through electromagnetic interactions has a long history. Low-energy theorems (LETs) successfully described charged pion photoproduction but initially failed for the $\gamma p \to \pi^0 p$ process [2–7]. Bernard *et al.* resolved these discrepancies by incorporating chiral perturbation theory (ChPT) corrections [8–13], advancing our understanding of QCD chiral dynamics, where quantum fluctuations (i.e., pion loops) are of prime importance. Increasing beam energies in recent electron-nucleon experiments have made it more challenging to probe pion production directly in the threshold region. The latest photoproduction data from MAMI, over a decade old [14], only cover energies above the second threshold, where the $\pi^+ n$ channel opens. For a recent review, see [15]. For electroproduction, where the photon carries nonzero four-momentum squared, the situation is less clear. While the extension of the LETs to electroproduction and the ChPT analyses of experimental data exist [16–20], discrepancies among different measurements and deviations from ChPT predictions persist [21], prompting further theoretical efforts [22–24]. Lattice QCD calculations offer a first-principles approach to predicting threshold pion

*Contact author: xu.feng@pku.edu.cn
†Contact author: ljin.luchang@gmail.com

Published by the American Physical Society under the terms of the Creative Commons Attribution 4.0 International license. Further distribution of this work must maintain attribution to the author(s) and the published article's title, journal citation, and DOI. Funded by SCOAP³.

electroproduction, enabling direct comparisons with experiment and ChPT. Such comparisons are essential for improving our understanding of chiral dynamics in QCD.

Weak pion production is crucial for neutrino oscillation experiments, where neutrino-nucleus interactions are a major source of systematic uncertainty. This impacts both intermediate-energy experiments like LBNF/DUNE [25], HyperK [26], and JUNO [27], as well as low-energy coherent neutrino scattering programs [28,29]. The DUNE Conceptual Design Report highlights that uncertainties exceeding 1% for signals and 5% for backgrounds could significantly reduce sensitivity to CP violation and the neutrino mass hierarchy [25]. A significant portion of the DUNE neutrino flux lies above the pion production threshold, making precise theoretical understanding of pion production processes crucial. To achieve few-percent overall cross-section uncertainties, these processes must be understood at the 10% level [30]. New data on neutrino scattering off proton or deuteron targets would provide valuable constraints. Theoretically, LETs are detailed in [31]. While lattice QCD can offer crucial insights, current studies of matrix elements involving nucleon-pion rescattering states remain exploratory compared to axial form factor calculations. Theoretical and computational advances are required to deliver results with fully quantified uncertainties.

Lattice QCD calculations involving baryonic multihadron states are inherently challenging due to increased system complexity, poorer signal-to-noise ratios, and potentially significant excited-state contamination. Recent studies have explored the excited-state contamination in nucleon matrix elements [32–37]. Building on our previous studies of nucleon electric polarizabilities [38] and subtraction functions in forward Compton scattering [39], we present a lattice QCD calculation of $\gamma^* N \to N\pi$, $W^* N \to N\pi$, and $Z^* N \to N\pi$ matrix elements at the pion production threshold. Using two gauge ensembles near the physical pion mass but with different lattice spacings, we extract the multipole amplitudes E_{0+} and L_{0+} from pion electroproduction and $L_{0+}^{(W)}$, M_{0+}, and H_{0+} from weak production. A detailed comparison is conducted between lattice results, experimental data and LET predictions.

Multipole amplitudes at the pion production threshold—Consider the process of $\gamma^*(k) + N(p_1) \to N(p_2) + \pi(q)$, where N represents a nucleon (proton or neutron), π denotes a pion, and γ^* is a virtual photon with spacelike momenta if $k^2 < 0$. Replacing γ^* with W^* or Z^* transforms the electromagnetic process to a weak one. The transition matrix elements for the electromagnetic and axial weak current are given by

$$\begin{aligned} \mathcal{J}_\mu^{em} &= \langle N\pi | J_\mu^{em}(0) | N \rangle, \\ \mathcal{J}_\mu^{W(Z),A} &= \langle N\pi | J_\mu^{W(Z),A}(0) | N \rangle, \end{aligned} \tag{1}$$

where the currents are defined as

$$\begin{aligned} J_\mu^{em} &= e\left(\frac{2}{3}\bar{u}\gamma_\mu u - \frac{1}{3}\bar{d}\gamma_\mu d\right), \\ J_\mu^{W,A} &= -\frac{g_2}{2\sqrt{2}}\bar{d}\gamma_\mu\gamma_5 u, \\ J_\mu^{Z,A} &= -\frac{g_2}{4\cos\theta_W}(\bar{u}\gamma_\mu\gamma_5 u - \bar{d}\gamma_\mu\gamma_5 d). \end{aligned} \tag{2}$$

Here, u, d are the up and down quark fields, e and g_2 are the electromagentic and weak $\mathrm{SU}(2)_L$ coupling constants, and θ_W is the Weinberg angle. The minus sign associated with the axial vector current reflects the $V-A$ structure of the weak interaction.

In the $N\pi$ center-of-mass frame at threshold ($\vec{q} = \vec{p}_2 = \vec{0}$), the electromagnetic current matrix element can be expressed in terms of two S-wave multipole amplitudes, E_{0+} and L_{0+} [18]

$$[\vec{\mathcal{J}}^{em}]_{s',s} = \alpha_m \xi_{s'}^\dagger \left\{ L_{0+}\hat{k}(\vec{\sigma}\cdot\hat{k}) + E_{0+}\left[\vec{\sigma} - \hat{k}(\vec{\sigma}\cdot\hat{k})\right] \right\} \xi_s, \tag{3}$$

where $\alpha_m = 8\pi\, i(m + M_\pi)$, with m and M_π being the masses of the nucleon and pion, respectively. $\xi_{s',s}$ are two-component Pauli spinors for the nucleon, normalized as $\xi_{s'}^\dagger \xi_s = \delta_{s,s'}$, where s and s' denote the nucleon spin in the initial and final states. The multipole amplitude E_{0+} characterizes the transverse coupling of the virtual photon to the nucleon spin, while L_{0+} characterizes the longitudinal coupling. Equation (3) applies for $\vec{k} \neq \vec{0}$. At $\vec{k} = \vec{0}$, L_{0+}, and E_{0+} are equal in magnitude [18], simplifying the expression to $[\vec{\mathcal{J}}^{em}]_{s',s} = \alpha_m E_{0+} \xi_{s'}^\dagger \vec{\sigma} \xi_s$. When $\vec{k} \neq \vec{0}$, L_{0+} can also be extracted from the time component of the current, $\mathcal{J}_0^{em}$, using the Ward identity

$$[\mathcal{J}_0^{em}]_{s',s} = \alpha_m \frac{|\vec{k}|}{k_0} \xi_{s'}^\dagger (\vec{\sigma}\cdot\hat{k}) \xi_s L_{0+}. \tag{4}$$

For weak interactions mediated by the W boson, the axial weak current matrix element is expressed as [31]

$$\begin{aligned} [\mathcal{J}_0^{W,A}]_{s',s} &= \alpha_m \xi_{s'}^\dagger \xi_s \left(L_{0+}^{(W)} + \frac{k_0}{m} H_{0+} \right), \\ [\vec{\mathcal{J}}^{W,A}]_{s',s} &= \alpha_m \xi_{s'}^\dagger \left(\frac{\vec{k}}{m} H_{0+} - i(\vec{\sigma}\times\hat{k}) M_{0+} \right) \xi_s, \end{aligned} \tag{5}$$

where $L_{0+}^{(W)}$, H_{0+}, and M_{0+} are the S-wave multipole amplitudes. To distinguish between electromagnetic and weak transitions, the superscript (W) is added to L_{0+} for the weak transition. For the Z boson, the matrix elements are defined analogously, with the superscript W replaced by Z. These multipole amplitudes can also be expressed in the isospin basis. The relationships between the multipole amplitudes in the physical and isospin bases are provided in the Supplemental Material [40].

Spin projection for correlation functions—The nucleon-pion operators $O_{N\pi}^{I,I_z}$ with isospin $I = \frac{1}{2}$ and $\frac{3}{2}$ are constructed

using the isospin-triplet operator for the pion, O_π^{I,I_z}, and the doublet operator for the nucleon, O_N^{I,I_z}, with appropriate coefficients. More details of the construction are given in the Supplemental Material [40].

To simplify the analysis, we first apply the projection operator $\mathcal{P}_+ = [(1+\gamma_0)/2]$ to the nucleon field, reducing it to a two-component field. Consequently, the spin structure of the correlation functions and matrix elements is analyzed within a 2×2 spin space. The overlap of the interpolating operators O_N^{I,I_z} and $O_{N\pi}^{I,I_z}$ with the nucleon and nucleon-pion ground state is expressed as

$$\begin{aligned}\langle 0|O_N^{I,I_z}(\vec{p},t)|N^{I,I_z},\vec{p},s\rangle_V &= L^3 Z_{N,L}(\vec{p}) e^{-Et}\xi_s,\\ \langle 0|O_{N\pi}^{I,I_z}(\vec{p},t)|(N\pi)^{I,I_z},G_1^-,s\rangle_V &= L^3 Z^I_{N\pi,L}(\vec{p}) e^{-E^I_{N\pi}t}\xi_s,\end{aligned} \quad (6)$$

where the operators $O_N^{I,I_z}(\vec{p},t)$ and $O_{N\pi}^{I,I_z}(\vec{p},t)$ are defined as

$$\begin{aligned}O_N^{I,I_z}(\vec{p},t) &= \sum_{\vec{x}} O_N^{I,I_z}(\vec{x},t)e^{i\vec{p}\cdot\vec{x}},\\ O_{N\pi}^{I,I_z}(\vec{p},t) &= \frac{1}{N_R}\sum_{\hat{R}\in O_h}\sum_{\vec{x},\vec{y}} O_{N\pi}^{I,I_z}(\vec{x},\vec{y},t)e^{i\hat{R}\vec{k}\cdot(\vec{x}-\vec{y})},\end{aligned} \quad (7)$$

with $N_R = \sum_{\hat{R}\in O_h} 1$, and $\hat{R}$ is an element of the hypercubic group O_h, which describes the rotational symmetry in a finite volume. The operator $O_{N\pi}^{I,I_z}(\vec{p},t)$ is defined in the center-of-mass frame, with $\vec{p}$ serving only as an indicator of the operator construction. The coordinates $\vec{x}$ and $\vec{y}$ correspond to the spatial positions of the nucleon and pion operators, respectively. The factor L^3 accounts for the finite volume, where L represents the lattice size. The subscript V denotes the states in a finite volume. E and $E^I_{N\pi}$ represent the energies of the nucleon and nucleon-pion states, respectively.

The G_1^- representation is a two-dimensional irreducible representation of O_h, with basis states labeled by the index s, which remain consistent with the spin index in the infinite-volume limit. The finite-volume states are normalized by

$$\begin{aligned}{}_V\langle N^{I,I_z'},\vec{p}',s'|N^{I,I_z},\vec{p},s\rangle_V &= 2EL^3\delta_{I_z,I_z'}\delta_{s,s'}\delta_{\vec{p},\vec{p}'},\\ {}_V\langle (N\pi)^{I,I_z'},G_1^-,s'|(N\pi)^{I,I_z},G_1^-,s\rangle_V &= 2E^I_{N\pi}L^3\delta_{I_z,I_z'}\delta_{s,s'}.\end{aligned} \quad (8)$$

The correlation functions are constructed as

$$\begin{aligned}C_{N\pi JN}(t_f,t_J,t_i) &= \langle O_{N\pi}^{I'',I_z''}(\vec{0},t_f)\tilde{J}_\mu^{I',I_z'}(\vec{k},t_J)\bar{O}_N^{I,I_z}(\vec{p},t_i)\rangle,\\ C_{N\pi}(t_f,t_i) &= \langle O_{N\pi}^{I,I_z}(\vec{0},t_f)\bar{O}_{N\pi}^{I,I_z}(\vec{0},t_i)\rangle,\\ C_N(t_f,t_i) &= \langle O_N^{I,I_z}(-\vec{p},t_f)\bar{O}_N^{I,I_z}(\vec{p},t_i)\rangle.\end{aligned} \quad (9)$$

According to Eq. (6), a typical operator O^{I,I_z} acts as an annihilation operator, removing a state with isospin (I,I_z). However, the same operator can also act as a creation operator, generating a state with isospin $(I,-I_z)$. To clarify this distinction, we introduce the notation $\tilde{O}^{I,-I_z}$ to represent O^{I,I_z} when it functions as a creation operator. This convention similarly applies to the current operator. By using $\tilde{J}_\mu^{I',I_z'}$ in the correlation function, we ensure that the isospin relation $I_z + I_z' = I_z''$ holds. Specifically, we set $(I_z,I_z') = (\frac{1}{2},0)$. Other choices of (I_z,I_z') can be related to this setup through the Wigner-Eckart theorem. Additionally, the current's momentum $\vec{k}$ satisfies the momentum conservation condition $\vec{p}+\vec{k}=\vec{0}$.

For the correlation functions $C_N(t_f,t_i)$ and $C_{N\pi}(t_f,t_i)$, at large time separation $t_f - t_i$, we obtain

$$\begin{aligned}\frac{1}{2}\mathrm{Tr}[C_N(t_f,t_i)] &= L^3\frac{Z_{N,L}(\vec{p})^2}{2E}e^{-E(t_f-t_i)},\\ \frac{1}{2}\mathrm{Tr}[C_{N\pi}(t_f,t_i)] &= L^3\frac{Z^I_{N\pi,L}(\vec{0})^2}{2E^I_{N\pi}}e^{-E^I_{N\pi}(t_f-t_i)}.\end{aligned} \quad (10)$$

For the correlation function $C_{N\pi JN}$, we use $\vec{C}$ and C^0 to distinguish its spatial and temporal components, and denote vector and axial-vector current insertions by $J = V$ and A, respectively. Before applying the trace operator, we first express

$$C_{N\pi JN} = \alpha_{N\pi JN}\sum_{s',s}\xi_{s'}[\mathcal{J}]_{s',s}\xi_s^\dagger, \quad (11)$$

where the coefficient is given by

$$\alpha_{N\pi JN} = L^3\frac{Z^I_{N\pi,L}(\vec{0})}{2E^I_{N\pi}}e^{-E_{N\pi}(t_f-t_J)}\frac{Z_{N,L}(\vec{p})}{2E}e^{-E(t_J-t_i)}. \quad (12)$$

To extract the five multipole amplitudes, we define the following spin projection operators

$$\begin{aligned}\mathcal{P}_{L_{0+}} &= \frac{k_0}{|\vec{k}|}(\hat{k}\cdot\vec{\sigma}), \quad \vec{\mathcal{P}}_{E_{0+}} = \frac{1}{2}(\vec{\sigma}-(\hat{k}\cdot\vec{\sigma})\hat{k}),\\ \vec{\mathcal{P}}_{H_{0+}} &= \frac{m}{|\vec{k}|}\hat{k}, \quad \mathcal{P}_{L^{(W)}_{0+},H_{0+}} = 1, \quad \vec{\mathcal{P}}_{M_{0+}} = \frac{i}{2}(\vec{\sigma}\times\hat{k}).\end{aligned} \quad (13)$$

These projection operators are applied to correlation functions to extract the multipole amplitudes. For example,

$$\begin{aligned}&\frac{1}{N_R}\sum_{\hat{R}\in O_h}\frac{1}{2}\mathrm{Tr}[\mathcal{P}_{L_{0+}}\cdot C^0_{N\pi VN}]|_{\hat{R}\vec{k}}\\ &\quad = (2\mu_{N\pi})^{-\frac{1}{2}}f_{LL}^{-\frac{1}{2}}\alpha_{N\pi JN}\alpha_m L_{0+},\end{aligned} \quad (14)$$

where f_{LL} is the Lellouch-Lüscher factor that relates the finite-volume state to the infinite-volume one, and $\mu_{N\pi} = (mM_\pi/E_{N\pi})$ is the reduced mass of the nucleon-pion system. Other multipole amplitudes can be extracted by applying the corresponding spin projection operators to the relevant correlation functions, as summarized in Table I. These projection operators are valid for $\vec{k}\neq\vec{0}$. For $\vec{k}=\vec{0}$, E_{0+} can be extracted by applying $\vec{\mathcal{P}}_{E_{0+}} = \vec{\sigma}/3$ to $\vec{C}_{N\pi VN}$.

Applying the projection operator $\vec{\mathcal{P}}_{L_{0+}} = (\hat{k}\cdot\vec{\sigma})\hat{k}$ to $\vec{C}_{N\pi VN}$ can also extract L_{0+}, but $\mathcal{P}_{L_{0+}}$ is preferred as it

TABLE I. The correspondence between spin projection operators, correlation functions, and multipole amplitudes.

$\mathcal{P}_{L_{0+}}$	$\vec{\mathcal{P}}_{E_{0+}}$	$\vec{\mathcal{P}}_{H_{0+}}$	$\mathcal{P}_{L_{0+}^{(W)},H_{0+}}$	$\vec{\mathcal{P}}_{M_{0+}}$
$C^0_{N\pi VN}$	$\vec{C}_{N\pi VN}$	$\vec{C}_{N\pi AN}$	$C^0_{N\pi AN}$	$\vec{C}_{N\pi AN}$
L_{0+}	E_{0+}	H_{0+}	$L_{0+}^{(W)} + (k_0/m)H_{0+}$	M_{0+}

reduces systematic effects. For instance, if the lattice size is tuned such that $k_0 = 0$, L_{0+} should vanish, yet $\vec{\mathcal{P}}_{L_{0+}}$ fails to ensure this due to systematic uncertainties. In our Letter, the factor $k_0/|\vec{k}|$ takes small values of 0.376, 0.170, and 0.063, which helps suppress systematic effects when using $\mathcal{P}_{L_{0+}}$. Conversely, we observe significant excited-state contamination when using $\vec{\mathcal{P}}_{L_{0+}}$, leading us to adopt $\mathcal{P}_{L_{0+}}$ exclusively. Further details on the design of spin operators and the discussion of Lellouch-Lüscher factor are provided in the Supplemental Material [40].

Operator optimization—To reduce excited-state contamination, we use $O^{I,I_z}_{N\pi}(\vec{p},t)$ with the four lowest momentum modes

$$\frac{\vec{p}}{2\pi/L} = (0,0,0),(0,0,1),(0,1,1),(1,1,1). \quad (15)$$

These operators are denoted as $O^{(n)}_{N\pi}$, where $n = 1, 2, 3, 4$ corresponds to increasing momentum modes. For simplicity, we have omitted the isospin index. Using these operators, we construct a 4×4 correlation function matrix with elements given by

$$\mathcal{M}^{n,m}_{N\pi}(t_f - t_i) = \frac{1}{2}\mathrm{Tr}\langle O^{(n)}_{N\pi}(t_f)\bar{O}^{(m)}_{N\pi}(t_i)\rangle. \quad (16)$$

The four lowest states are defined as $|N\pi, G_1^-, s, n\rangle_V$ with $n = 1, 2, 3, 4$.

By solving the generalized eigenvalue problem (GEVP), we construct optimized $N\pi$ operators as

$$\tilde{O}_{N\pi} = O^{(1)}_{N\pi} + c_2 O^{(2)}_{N\pi} + c_3 O^{(3)}_{N\pi} + c_4 O^{(4)}_{N\pi}, \quad (17)$$

where the coefficients c_m are determined using the standard GEVP procedure [44,45]. Assuming that the lowest four states dominate the correlation function matrix, with higher excited-state contributions being negligible compared to the statistical noise, the coefficients c_m can be considered to satisfy the condition

$$\langle 0|\tilde{O}_{N\pi}|N\pi, G_1^-, s, n\rangle_V = 0, \quad \text{for } n = 2,3,4. \quad (18)$$

For the nucleon operator with nonzero momentum $\vec{p}$, parity is no longer a good quantum number, allowing mixing with $N\pi$ operators of the same momentum. We consider three operators

$$O^{(1)}_N = O_N(\vec{p}), \qquad O^{(2)}_N = (\hat{p}\cdot\vec{\sigma})O_N(\vec{p})O_\pi(\vec{0}),$$
$$O^{(3)}_N = (\hat{p}\cdot\vec{\sigma})O_N(\vec{0})O_\pi(\vec{p}), \quad (19)$$

using which, we construct the correlation function matrix

$$\mathcal{M}^{n,m}_N(t_f - t_i) = \frac{1}{2}\mathrm{Tr}\langle O^{(n)}_N(t_f)\bar{O}^{(m)}_N(t_i)\rangle. \quad (20)$$

It is explained in the Supplemental Material [40] why this matrix is suitable for GEVP analysis [40]. By solving the GEVP, we obtain the optimized nucleon operator

$$\tilde{O}_N = O^{(1)}_N + d_2 O^{(2)}_N + d_3 O^{(3)}_N, \quad (21)$$

where the coefficients $d_{2,3}$ satisfy

$$\langle 0|\tilde{O}_N|N(\vec{0})\pi(\vec{p})\rangle_V = 0, \quad \langle 0|\tilde{O}_N|N(\vec{p})\pi(\vec{0})\rangle_V = 0. \quad (22)$$

We construct the correlation function using the optimized operators

$$\tilde{C}_{N\pi JN}(t_f,t_J,t_i) = \langle \tilde{O}_{N\pi}(t_f)\tilde{J}_\mu(t_J)\bar{\tilde{O}}_N(t_i)\rangle, \quad (23)$$

where we include only terms from $C_{N\pi JN}$ and those proportional to the coefficients $c_{2,3,4}$ and $d_{2,3}$. Terms involving products of $c_m d_n$ are treated as higher-order corrections and neglected. A challenge in computing correlation functions like $\langle O^{(1)}_{N\pi}(t_f)\tilde{J}_\mu(t_J)\bar{O}^{(n)}_N(t_i)\rangle$ for $n = 2, 3$ is the evaluation of five-point correlation functions. Since the disconnected diagrams encapsulate the contributions from $\langle N(\vec{0})|N(\vec{0})\rangle\langle\pi(\vec{0})|\tilde{J}_\mu|\pi(\vec{p})\rangle$ and $\langle N(\vec{0})|\tilde{J}_\mu|N(\vec{p})\rangle\langle\pi(\vec{0})|\pi(\vec{0})\rangle$, which are enhanced by a factor of spatial volume of the lattice, they dominate the five-point correlation functions based on the factorization approximation

$$\langle N(\vec{0})\pi(\vec{0})|\tilde{J}_\mu|N(\vec{0})\pi(\vec{p})\rangle \approx \langle N(\vec{0})|N(\vec{0})\rangle\langle\pi(\vec{0})|\tilde{J}_\mu|\pi(\vec{p})\rangle,$$
$$\langle N(\vec{0})\pi(\vec{0})|\tilde{J}_\mu|N(\vec{p})\pi(\vec{0})\rangle \approx \langle N(\vec{0})|\tilde{J}_\mu|N(\vec{p})\rangle\langle\pi(\vec{0})|\pi(\vec{0})\rangle.$$

Therefore, we compute only the disconnected contributions as approximations to the challenging five-point functions, which is feasible within current lattice QCD studies. Though certain simplifications have been made, they mainly affect corrections for excited-state contamination and are therefore acceptable. Future work to develop methods for handling five-point correlation functions is beneficial.

Numerical analysis—We used two $2+1$-flavor domain wall fermion ensembles, 24D and 32Df, from the RBC-UKQCD Collaboration [46], which have similar pion masses [142.6(3) and 142.9(7) MeV [47]], comparable spatial volumes ($L = 4.6$ fm), the same discretization but different lattice spacings [$a^{-1} = 1.023(2)$ and 1.378(5) GeV]. For each configuration, we generate 1024 point-source and 1024 smeared-source propagators at randomly chosen spatiotemporal locations to compute the correlation functions, using the random sparsening-field technique [48,49]. Smeared nucleon operators and local current operators are used, with renormalization factors provided in Ref. [50]. Additional details on

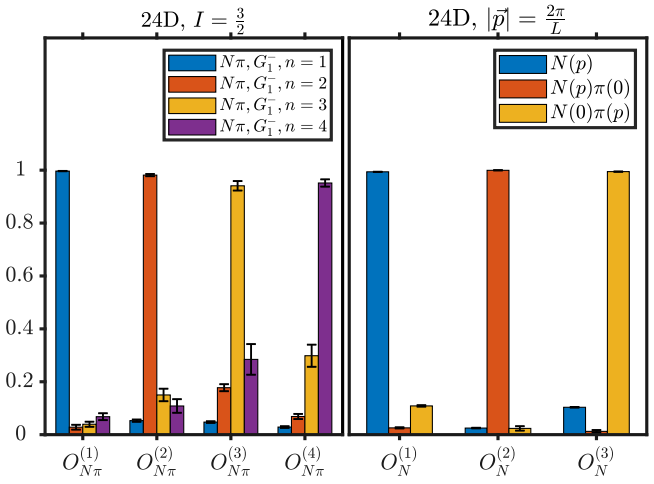

FIG. 1. The overlap of the operators $O_{N\pi}^{(n)}$ for $n = 1, 2, 3, 4$ (left) and $O_N^{(n)}$ for $n = 1, 2, 3$ (right) with the eigenstates from the GEVP analysis.

the computation of four-point correlation functions can be found in Refs. [38,51,52].

Taking the 24D ensemble and the $I = 3/2$ $N\pi$ system as an example, we show the GEVP analysis results in the left panel of Fig. 1. For each operator $O_{N\pi}^{(n)}$, we plot its overlap with the state $|N\pi, G_1^-, s, m\rangle$, defined as $c_{n,m} = |\langle 0|O_{N\pi}^{(n)}|N\pi, G_1^-, s, m\rangle_V|$, normalized by $\sqrt{\sum_m c_{n,m}^2}$. Similarly, for the nucleon system with momentum $|\vec{p}| = (2\pi/L)$, the right panel of Fig. 1 presents the corresponding GEVP results. The overlaps with excited states for the operators $O_{N\pi}^{(1)}$ and $O_N^{(1)}$ are about 5% and 10%, respectively. Although these overlaps are small, eliminating excited-state contamination remains crucial, as discussed below.

Using Eqs. (10) and (14), we extract the effective multipole amplitude for given time separations $t_{N\pi} - t_J$ and $t_J - t_N$. Since the initial and final state operators differ significantly, we analyze their time dependence separately. We first fix $t_N - t_J$ and compute the multipole amplitude as a function of $t_{N\pi} - t_J$ to assess excited-state contamination on the $N\pi$ side. By fitting this dependence, we obtain an effective multipole amplitude dependent only on $t_N - t_J$. We then examine excited-state contamination on the N side and extract the final multipole amplitude by fitting its $t_N - t_J$ dependence.

We take H_{0+} and L_{0+} as examples to illustrate the impact of the GEVP correction on the $N\pi$ and N sides, respectively. Figure 2 shows H_{0+} as a function of $t_{N\pi} - t_J$ for $t_J - t_N = 0.58$ fm, comparing results with and without GEVP corrections. Here, "with GEVP" refers to the use of the optimized operator $\tilde{O}_{N\pi}(t)$, which retains both the $C_{N\pi JN}$ term and terms proportional to $c_{2,3,4}$, whereas "without GEVP" omits the $c_{2,3,4}$ corrections. As the coupling of $O_{N\pi}^{(1)}$ with excited states is weak, the GEVP

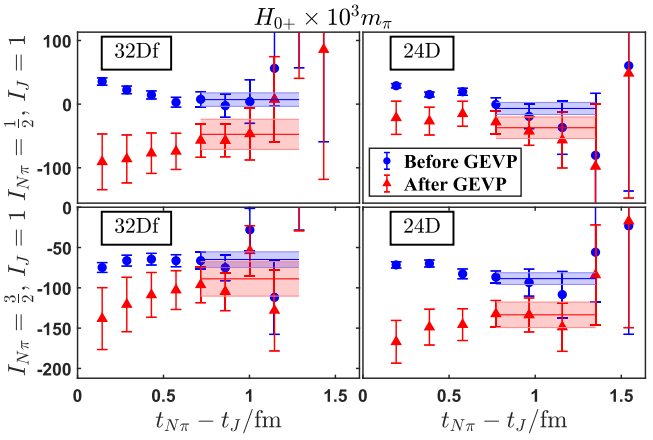

FIG. 2. Effective multipole amplitude H_{0+} as a function of $t_{N\pi} - t_J$ for $t_J - t_N = 0.58$ fm.

corrections are not highly significant as shown in Fig. 2. However, they still cause a shift by around 1–3σ.

Figure 3 compares L_{0+} as a function of $t_J - t_N$ with and without GEVP corrections on the N side. Here, the $t_J - t_N$ dependence is analyzed using data that include the $c_{2,3,4}$ corrections. The terms with GEVP and without GEVP indicate whether the $d_{2,3}$ terms are included. The GEVP correction is crucial: before GEVP, significant excited-state contamination is visible at small $t_J - t_N$, whereas after correction, a clearer plateau emerges. The difference can reach 6σ in the more precise 24D data. Since nucleon operators with nonzero momenta are widely used in lattice calculations, such as for parton distribution functions, removing excited-state contamination using techniques like GEVP is essential. It is worth noting that GEVP optimization has only a mild effect on the single-nucleon two-point correlation function $C_N(t_f, t_i)$. However, for matrix elements extracted from $C_{N\pi JN}(t_f, t_J, t_i)$, the impact of GEVP is significant. A more detailed discussion is

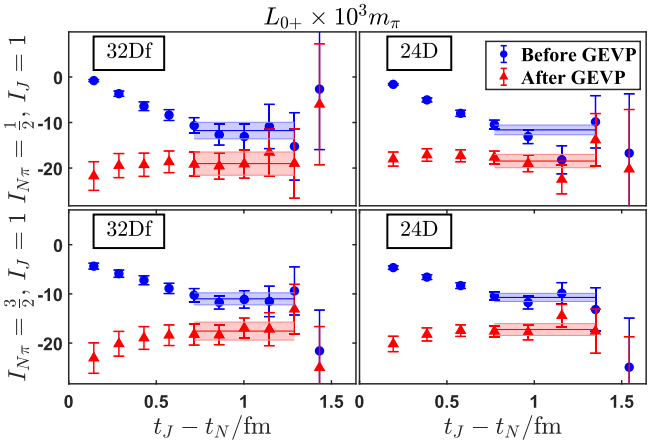

FIG. 3. Effective multipole amplitude L_{0+} as a function of $t_J - t_N$, obtained from a fit using GEVP-corrected data on the $N\pi$ side to analyze the time dependence on the N side, both before and after GEVP correction on the N side.

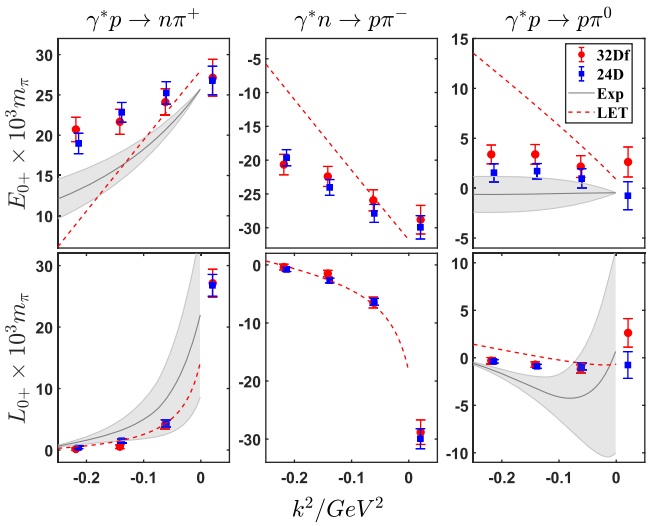

FIG. 4. Comparison between lattice results for L_{0+} and E_{0+} with those extracted from experimental data and predicted by LETs. The lattice value of L_{0+} at $k^2 = M_\pi^2$ is determined by enforcing the condition $L_{0+} = E_{0+}$ at $\vec{k} = \vec{0}$. Experimental data and LET predictions are available in the spacelike region ($k^2 < 0$), as reported in Refs. [18,53].

provided in the Supplemental Material [40]. Figures illustrating the fitting quality for other multipole amplitudes are also included in [40].

Results and conclusion—Figure 4 shows the momentum dependence of the multipole amplitudes obtained from fits to both the $t_{N\pi} - t_J$ and $t_J - t_N$ dependences. The amplitudes L_{0+} and E_{0+} are presented in the physical basis, allowing for a direct comparison of the lattice results with extractions from experimental data and predictions from LETs, including $O[(M_\pi/m)^2]$ corrections [18]. Lattice results for other multipole amplitudes in the isospin basis are provided in the Supplemental Material [40]. Several partial-wave analyses based on experimental data exist [53–59]. In this Letter, we compare our results with the most recent analysis within a coupled-channel framework [53]. Note, however, this analysis does not incorporate matching to the ChPT amplitude at low energies and momenta, and only proton target data are analyzed, as the neutron in the initial state is bound in a deuteron or ^{3}He, making the theoretical interpretation less clean.

In Fig. 4, the lattice data exhibit a similar trend to both experimental analyses and LET predictions but align more closely with the experimental results while deviating more from LETs. This discrepancy arises because LETs omit higher-order corrections within the framework of ChPT. Although some differences exist between the lattice and experimental results, the large uncertainties in the experimental data imply that the lattice and experimental results are either consistent or deviate by around 2–3σ. Additionally, some deviations between the two lattice ensembles can be observed. While these differences may arise from lattice artifacts, they could also result from statistical fluctuations. Further investigation into these effects, using larger statistics and additional lattice spacings, would be a valuable direction for future studies. Improved precision in both lattice calculations and experiments will enable mutual validation and deepen our understanding of pion production from a nucleon, a fundamental quantum fluctuation process.

As the first lattice QCD study of pion production, our approach to spin projection and multiple operator construction extends techniques developed to study excited-state effects in nucleon observables and holds promise for the eventual calculation of shallow inelastic neutrino-nucleon scattering.

Acknowledgments—X. F. and L. C. J. gratefully acknowledge many helpful discussions with our colleagues from the RBC-UKQCD Collaborations. We would like to express our gratitude to T.-S. H. Lee and I. Strakovsky for the discussion on partial-wave analysis of the experimental data. X. F., Y. S. G., C. L., and Z. L. Z. were supported in part by NSFC of China under Grants No. 12125501, No. 12293060, No. 12293063, and No. 12141501. L. C. J. acknowledges support by DOE Office of Science Early Career Award No. DE-SC0021147 and DOE Award No. DE-SC0010339. The work of U.-G. M. was supported in part by the CAS President's International Fellowship Initiative (PIFI) (Grant No. 2025PD0022) and by the Deutsche Forschungsgemeinschaft (DFG, German Research Foundation) as part of the CRC 1639 NuMeriQS – Project No. 511713970. The research reported in this work was carried out using the computing facilities at Chinese National Supercomputer Center in Tianjin. It also made use of computing and long-term storage facilities of the USQCD Collaboration, which are funded by the Office of Science of the U.S. Department of Energy.

Data availability—The data supporting this study's findings are available within the article.

[1] A. M. Bernstein, M. W. Ahmed, S. Stave, Y. K. Wu, and H. R. Weller, Annu. Rev. Nucl. Part. Sci. **59**, 115 (2009).
[2] R. J. Walker, T. R. Palfrey, R. O. Haxby, and B. M. K. Nefkens, Phys. Rev. **132**, 2656 (1963).
[3] V. Rossi *et al.*, Nuovo Cimento A **13**, 59 (1973).
[4] M. Salomon, D. F. Measday, J. M. Poutissou, and B. C. Robertson, Nucl. Phys. **A414**, 493 (1984).
[5] E. Mazzucato *et al.*, Phys. Rev. Lett. **57**, 3144 (1986).
[6] R. Beck, F. Kalleicher, B. Schoch, J. Vogt, G. Koch, H. Stroher, V. Metag, J. C. McGeorge, J. D. Kellie, and S. J. Hall, Phys. Rev. Lett. **65**, 1841 (1990).
[7] D. Drechsel and L. Tiator, J. Phys. G **18**, 449 (1992).
[8] V. Bernard, N. Kaiser, J. Gasser, and U.-G. Meißner, Phys. Lett. B **268**, 291 (1991).
[9] V. Bernard, N. Kaiser, and U.-G. Meißner, Nucl. Phys. **B383**, 442 (1992).

[10] V. Bernard, N. Kaiser, and U.-G. Meißner, Z. Phys. C **70**, 483 (1996).
[11] V. Bernard, N. Kaiser, and U.-G. Meißner, Phys. Lett. B **378**, 337 (1996).
[12] V. Bernard, N. Kaiser, and U.-G. Meißner, Phys. Lett. B **383**, 116 (1996).
[13] V. Bernard, N. Kaiser, and U.-G. Meißner, Eur. Phys. J. A **11**, 209 (2001).
[14] D. Hornidge *et al.* (A2 and CB-TAPS Collaborations), Phys. Rev. Lett. **111**, 062004 (2013).
[15] U.-G. Meißner, Proc. Sci. CD2021 (**2024**) 001 [arXiv:2201.00341].
[16] V. Bernard, N. Kaiser, and U.-G. Meißner, Phys. Lett. B **282**, 448 (1992).
[17] V. Bernard, N. Kaiser, T. S. H. Lee, and U.-G. Meißner, Phys. Rev. Lett. **70**, 387 (1993).
[18] V. Bernard, N. Kaiser, T. S. H. Lee, and U.-G. Meißner, Phys. Rep. **246**, 315 (1994).
[19] V. Bernard, N. Kaiser, and U.-G. Meißner, Phys. Rev. Lett. **74**, 3752 (1995).
[20] V. Bernard, N. Kaiser, and U.-G. Meißner, Nucl. Phys. **A607**, 379 (1996); **A633**, 695(E) (1998).
[21] R. Lindgren, K. Chirapatimol, and L. C. Smith (Hall A Collaboration), Proc. Sci. CD12 (**2013**) 073.
[22] M. Hilt, B. C. Lehnhart, S. Scherer, and L. Tiator, Phys. Rev. C **88**, 055207 (2013).
[23] C. Fernandez-Ramirez and A. M. Bernstein, Phys. Lett. B **724**, 253 (2013).
[24] N. Rijneveen, A. M. Gasparyan, H. Krebs, and E. Epelbaum, Phys. Rev. C **106**, 025202 (2022).
[25] R. Acciarri *et al.* (DUNE Collaboration), arXiv:1512.06148.
[26] K. Abe *et al.* (Hyper-Kamiokande Collaboration), arXiv:1805.04163.
[27] F. An *et al.* (JUNO Collaboration), J. Phys. G **43**, 030401 (2016).
[28] D. Akimov *et al.* (COHERENT Collaboration), Science **357**, 1123 (2017).
[29] D. Akimov *et al.* (COHERENT Collaboration), Phys. Rev. Lett. **126**, 012002 (2021).
[30] L. A. Ruso *et al.*, arXiv:2203.09030.
[31] V. Bernard, N. Kaiser, and U. G. Meissner, Phys. Lett. B **331**, 137 (1994).
[32] L. Barca, G. Bali, and S. Collins, Phys. Rev. D **107**, L051505 (2023).
[33] A. V. Grebe and M. Wagman, Proc. Sci. LATTICE2023 (**2024**) 049 [arXiv:2312.00321].
[34] C. Alexandrou, G. Koutsou, Y. Li, M. Petschlies, and F. Pittler, Phys. Rev. D **110**, 094514 (2024).
[35] L. Barca, G. Bali, and S. Collins, Phys. Rev. D **111**, L031505 (2025).
[36] A. Hackl and C. Lehner, arXiv:2412.17442.
[37] S. Sasaki, Y. Aoki, K.-I. Ishikawa, Y. Kuramashi, K. Sato, E. Shintani, R. Tsuji, H. Watanabe, and T. Yamazaki (PACS Collaboration), Proc. Sci. LATTICE2024 (**2025**) 310.
[38] X.-H. Wang, Z.-L. Zhang, X.-H. Cao, C.-L. Fan, X. Feng, Y.-S. Gao, L.-C. Jin, and C. Liu, Phys. Rev. Lett. **133**, 141901 (2024).
[39] Y. Fu, X. Feng, L.-C. Jin, C. Liu, and S.-D. Wen, Phys. Rev. Lett. **134**, 071903 (2025).
[40] See Supplemental Material at http://link.aps.org/supplemental/10.1103/PhysRevLett.134.171904, which includes Refs. [41–43] additional information about the formula derivation and a detailed discussion of the numerical analysis.
[41] L. Lellouch and M. Lüscher, Commun. Math. Phys. **219**, 31 (2001).
[42] X. Feng, L.-C. Jin, X.-Y. Tuo, and S.-C. Xia, Phys. Rev. Lett. **122**, 022001 (2019).
[43] M. Lüscher, Commun. Math. Phys. **105**, 153 (1986).
[44] M. Luscher and U. Wolff, Nucl. Phys. **B339**, 222 (1990).
[45] B. Blossier, M. Della Morte, G. von Hippel, T. Mendes, and R. Sommer, J. High Energy Phys. 04 (2009) 094.
[46] T. Blum *et al.* (RBC and UKQCD Collaborations), Phys. Rev. D **93**, 074505 (2016).
[47] T. Lin, M. Bruno, X. Feng, L.-C. Jin, C. Lehner, C. Liu, and Q.-Y. Luo, arXiv:2411.06349.
[48] Y. Li, S.-C. Xia, X. Feng, L.-C. Jin, and C. Liu, Phys. Rev. D **103**, 014514 (2021).
[49] W. Detmold, D. J. Murphy, A. V. Pochinsky, M. J. Savage, P. E. Shanahan, and M. L. Wagman, Phys. Rev. D **104**, 034502 (2021).
[50] X. Feng, L. Jin, and M. J. Riberdy, Phys. Rev. Lett. **128**, 052003 (2022).
[51] Y. Fu, X. Feng, L.-C. Jin, and C.-F. Lu, Phys. Rev. Lett. **128**, 172002 (2022).
[52] P.-X. Ma, X. Feng, M. Gorchtein, L.-C. Jin, K.-F. Liu, C.-Y. Seng, B.-G. Wang, and Z.-L. Zhang, Phys. Rev. Lett. **132**, 191901 (2024).
[53] M. Mai, J. Hergenrather, M. Döring, T. Mart, U.-G. Meißner, D. Rönchen, and R. Workman (Jülich–Bonn–Washington Collaboration), Eur. Phys. J. A **59**, 286 (2023).
[54] H. Kamano, S. X. Nakamura, T. S. H. Lee, and T. Sato, Phys. Rev. C **88**, 035209 (2013).
[55] S. X. Nakamura, H. Kamano, and T. Sato, Phys. Rev. D **92**, 074024 (2015).
[56] H. Kamano, S. X. Nakamura, T. S. H. Lee, and T. Sato, Phys. Rev. C **94**, 015201 (2016).
[57] W. J. Briscoe, A. Schmidt, I. Strakovsky, R. L. Workman, and A. Svarc (SAID Group), Phys. Rev. C **108**, 065205 (2023).
[58] M. Mai, M. Döring, C. Granados, H. Haberzettl, Ulf-G. Meißner, D. Rönchen, I. Strakovsky, and R. Workman (Jülich-Bonn-Washington Collaboration), Phys. Rev. C **103**, 065204 (2021).
[59] M. Mai, M. Döring, C. Granados, H. Haberzettl, J. Hergenrather, Ulf-G. Meißner, D. Rönchen, I. Strakovsky, and R. Workman (Jülich-Bonn-Washington Collaboration), Phys. Rev. C **106**, 015201 (2022).